

A Method to Detect Abnormal Gas Dispersion Conditions in Flotation Machines

Luis Vinnett^{1,2,*} , Juan Yianatos^{1,2}, Claudio Acuña^{1,2} and Iván Cornejo¹ 

¹ Department of Chemical and Environmental Engineering, Universidad Técnica Federico Santa María, Valparaíso 2390123, Chile; juan.yianatos@usm.cl (J.Y.); claudio.acunap@usm.cl (C.A.); ivan.cornejo@usm.cl (I.C.)

² Automation and Supervision Centre for Mining Industry, CASIM, Universidad Técnica Federico Santa María, Valparaíso 2390123, Chile

* Correspondence: luis.vinnett@usm.cl

Abstract: This short communication presents a methodology to detect abnormal gas dispersion conditions in flotation machines. These abnormal conditions are characterized by the significant presence of cap-shaped bubbles. The approach considers the use of a bubble size analyzer to measure gas dispersion at industrial scale. The detection of abnormal conditions is critical when estimating bubble size by automated software. Otherwise, the estimates are significantly biased, since irregular bubbles are typically removed from the analysis. From the recorded images and the respective black and white representation, the variability of the shadow percentage caused by the bubbles in the vision field, abruptly increases in the presence of cap-shaped bubbles. Experimental conditions with coefficients of variation lower than 60–70% in the shadow percentage represent spherical and spherical-ellipsoidal regimes. In the former, automated bubble sizing software has proved to be sufficiently effective in obtaining reliable results. In the latter, different segmentation techniques have been proposed to obtain satisfactory results. Abnormal conditions are detected under coefficients of variation greater than 80% in the shadow percentage. The presence of cap-shaped bubbles causes inefficiencies in the collection of hydrophobic minerals in the pulp zone as well as disturbances in the separation stage (froth zone). Therefore, the detection of these irregular bubbles is suitable to provide feedback to flotation processes, allowing gas dispersion to be driven towards normal operating conditions.

Keywords: gas dispersion; flotation; bubble size; churn-turbulent regime; industrial measurements



Citation: Vinnett, L.; Yianatos, J.; Acuña, C.; Cornejo, I. A Method to Detect Abnormal Gas Dispersion Conditions in Flotation Machines. *Minerals* **2022**, *12*, 125. <https://doi.org/10.3390/min12020125>

Academic Editor: Lev Filippov

Received: 23 December 2021

Accepted: 20 January 2022

Published: 21 January 2022

Publisher's Note: MDPI stays neutral with regard to jurisdictional claims in published maps and institutional affiliations.



Copyright: © 2022 by the authors. Licensee MDPI, Basel, Switzerland. This article is an open access article distributed under the terms and conditions of the Creative Commons Attribution (CC BY) license (<https://creativecommons.org/licenses/by/4.0/>).

1. Introduction

Since the introduction of bubble size analyzers to characterize gas dispersion in flotation, several applications have been proposed to better understand and improve the process performance. For example, the relationship between gas dispersion and flotation kinetics [1–3], frother characterizations [4,5], collection and froth response relationships [6–8], among others. Most of these characterizations have been conducted at laboratory scale, in which flotation machines are typically operated in regimes dominated by spherical bubbles. Thus, the use of bubble samplers along with visual techniques for bubble size quantification has been successful in bubble size determination, due to the efficiency of software tools for circular detection [9,10]. However, industrial practice has shown deviations regarding spherical regimes, leading to bubble populations including ellipsoidal and cap-shaped bubbles (transitions to ellipsoidal and churn-turbulent regimes, respectively). The characterization of bubbles in the ellipsoidal regime has been subject to significant improvements due to the use of ellipse fitting by regression [9,11] or solidity together with moment-based axis quantifications [12,13]. However, these estimations are only successful when the percentage of bubbles observed in clusters is low or moderate-low. Cap-shaped bubbles are identified by their low circularities or solidities in 2D representation, and

automated software typically removes them from the image processing, biasing the bubble size estimation. However, complex clusters also present low circularities, which hinders the automated identification of irregular bubbles by image processing.

Large cap-shaped bubbles lead to detrimental performances in flotation due to a decrease in the available bubble surface and lower froth stability. Cap-shaped bubbles imply a higher Sauter mean diameter $D_{32} = \Sigma d_i^3 / \Sigma d_i^2$ and, therefore, a lower bubble surface area flux S_B , which has proved to be correlated with the collection rate constant [1–3]. In addition, these bubbles present higher terminal velocities [14,15], increasing the disturbances at the pulp–froth interface [16]. These disturbances increase entrainment and bubble coalescence throughout the froth, affecting the concentrate grades [16]. Although large cap-shaped bubbles result in negative effects on metallurgical performance, their detection has not received sufficient attention even though these conditions have been observed at industrial scale in flotation machines [9,17].

This short communication presents a methodology to detect significant presences of cap-shaped bubbles in flotation. The technique employs images acquired from the McGill bubble size analyzer (MBSA) [18] in their black and white representation. The variability of the shadow percentage obtained from the binary images is used as an indicator of abnormal gas dispersion conditions. The technique is tested with industrial data from mechanical flotation cells and columns.

2. Materials and Methods

Gas dispersion measurements were conducted in mechanical flotation cells (self-aerated and forced air) and flotation columns from different industrial concentrators. One hundred and two datasets were analyzed, with six of them corresponding to columns. Bubble populations were measured using the McGill bubble size analyzer shown in Figure 1a. The sampling tube was immersed about 15–30 cm below the pulp–froth interface to capture bubbles entering the froth. The chamber was fully filled with process water, which was displaced by the rising bubbles. A deflecting glass is installed in the MBSA to observe the bubbles in a 2D plane. A digital video camera (Canon GL2, Canon U.S.A. Inc., Lake Success, NY, USA) was used for image acquisition at a sampling rate of 30 frames per second. The image processing was carried out at time intervals of 1 s to avoid autocorrelation between the analyzed images. The visual field was set at 3.5 cm × 4.67 cm, leading to a resolution of 0.0729 mm/pxl. The MBSA was adapted to determine the local superficial gas rate J_G , which can be estimated by water volume displacement over time. The MBSA was completely sealed to avoid possible leaks in the industrial measurements, which is critical for reliable gas dispersion results.

A semi-automated image analysis tool based on the Image Processing Toolbox of Matlab (The MathWorks Inc., Natick, MA, USA) was used to obtain the bubble size distributions (BSD) and the statistical parameters from the bubble population, e.g., Sauter mean diameter. All images were analyzed based on their black and white representation. A hierarchical algorithm was implemented, which firstly allowed single bubble diameters to be estimated as equivalent ellipsoid diameter (volumetric). Simple clusters were automatically and sequentially segmented using Watershed and Hough transforms [10,19]. Complex clusters and irregular bubbles were manually estimated to reduce biases in the BSD estimations. Figure 1b illustrates the image processing procedure, in which bubbles highlighted by crosses were manually analyzed.

The shadow percentage σ_B was related to the D_{32} values to detect churn-turbulent conditions. This parameter corresponds to the number of black pixels divided by the total pixels in the processed images [20], as described by Equation (1). In the example of Figure 1b, σ_B is approximately 22%. The variability of σ_B showed an abrupt increase as gas dispersion transitioned to churn-turbulent regimes.

$$\sigma_B = 100 \times \frac{\Sigma(\text{Black Pixels})}{\Sigma(\text{Total Pixels})} \quad (1)$$

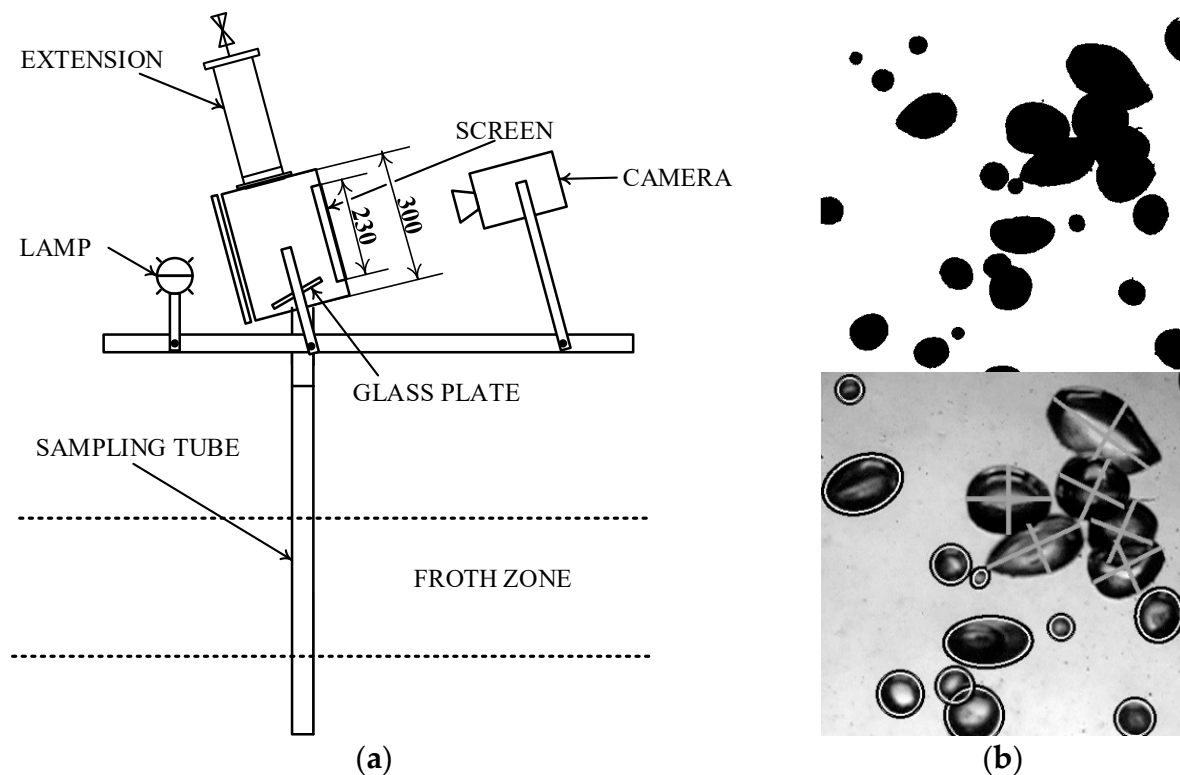


Figure 1. (a) McGill bubble size analyzer (modified from [20]) and (b) example of the image processing procedure (modified from [9]).

3. Results and Discussions

Figure 2 illustrates four randomly chosen binary images for experimental conditions under spherical and spherical-ellipsoidal regimes, and the transition to churn-turbulent regimes. These conditions correspond to mechanical flotation cells of 14 (self-aerated), 127 (forced-air), and 42.5 (self-aerated) m^3 , respectively. Spherical (Figure 2a) and spherical-ellipsoidal (Figure 2b) conditions presented stable shadow percentages with moderate variability with respect to the average. Conditions transitioning to churn-turbulent regimes presented peaks in the shadow percentage due to the random appearance of large cap-shaped bubbles, as shown in Figure 2c. Figure 3 presents the normalized shadow percentages for the three conditions shown in Figure 2. This normalized parameter represents instantaneous σ_B values divided by the average σ_B . The presence of cap-shaped bubbles increases the relative variability of σ_B in experimental conditions that transitioned to churn-turbulent regimes. Spherical and spherical-ellipsoidal conditions resulted in significantly lower relative variability, with normalized σ_B values oscillating around 1. Results from Figures 2 and 3 show that the presence of cap-shaped bubbles caused high instantaneous σ_B values, similar to spherical-ellipsoidal regimes with high gas hold-up. However, transitions to churn-turbulent regimes showed abrupt variations from low to high σ_B values. These variations were indirectly used to detect problems in gas dispersion. Normal conditions can be associated with a wide range of σ_B values, which were consistently steadier in all measurements.

Figure 4 shows the relationship between the Sauter mean diameters of the BSDs and coefficients of variation of the shadow percentage cv_{σ_B} . The coefficient of variation (or relative standard deviation) corresponds to the standard deviation divided by the mean value. Although noisy, the relative variability of σ_B explains part of the variability of D_{32} , which is observed as an increase in bubble size at higher cv_{σ_B} . Spherical ($D_{32} \lesssim 2.0$ mm) and spherical-ellipsoidal ($2.0 \text{ mm} \lesssim D_{32} \lesssim 5.0$ mm) regimes are observed with cv_{σ_B} lower than 70%. These experimental datasets correspond to typical operations in flotation, including flotation machines with $D_{32} > 3.0$ mm that are commonly associated with moderate-high

superficial gas rates [21]. Five experimental conditions presented transitions from ellipsoidal to churn-turbulent regimes. These datasets presented binary images as those shown in Figure 2c. As a result, the cv_{σ_B} values were consistently greater than 80%. Thus, high relative variability in the shadow percentage can be used as an indicator of transitions towards churn-turbulent regimes.

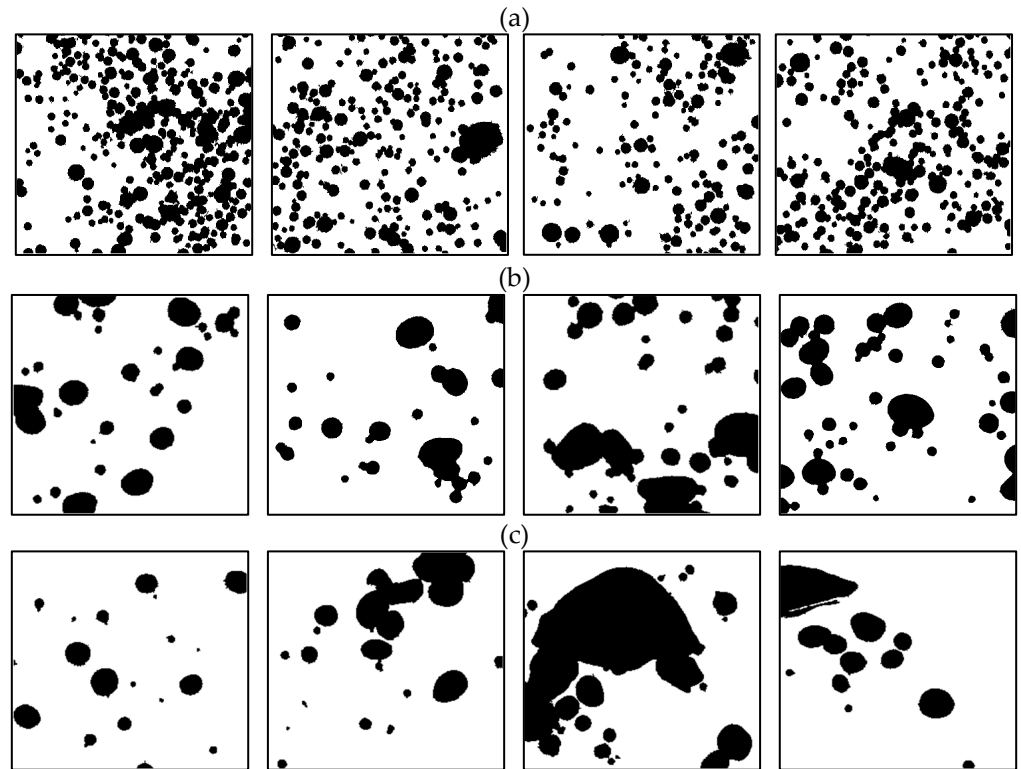


Figure 2. Examples of binary images for 3 experimental conditions: (a) spherical regime (14 m³ self-aerated flotation cell), (b) spherical–ellipsoidal regime (127 m³ forced-air flotation cell), and (c) transition to a churn-turbulent regime (42.5 m³ self-aerated flotation cell).

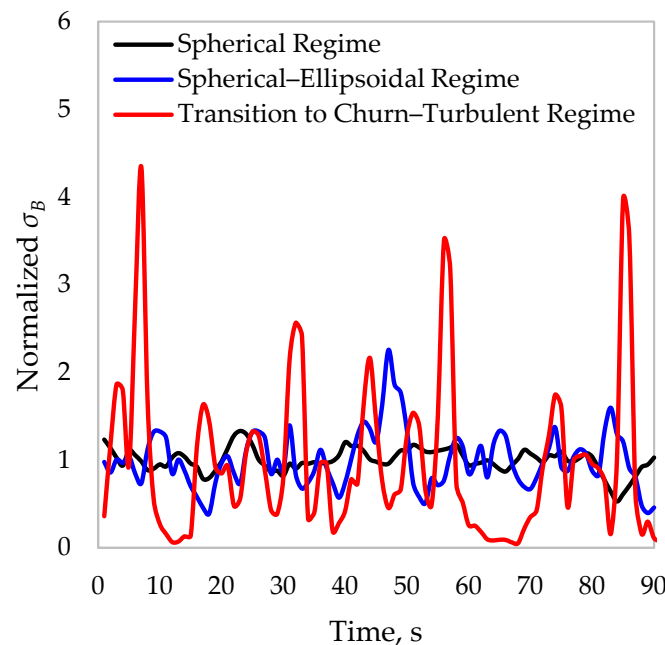


Figure 3. Normalized shadow percentages for the three conditions presented in Figure 2.

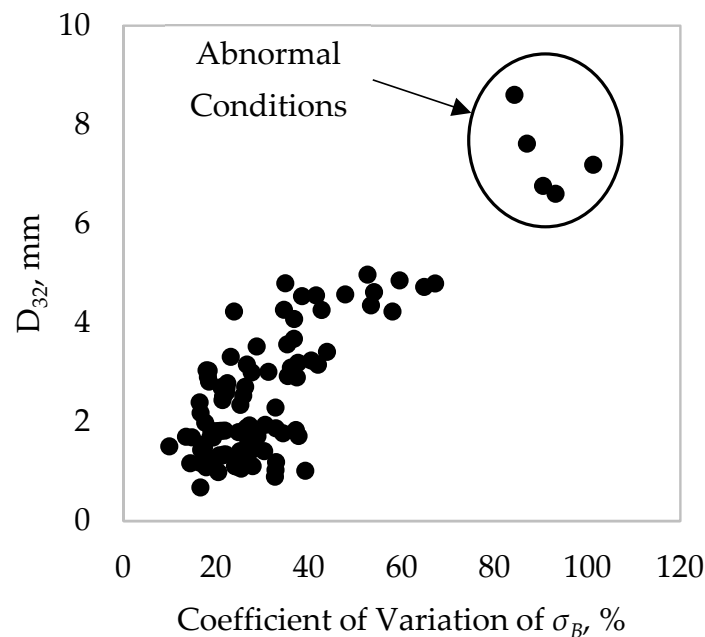


Figure 4. Sauter mean diameter versus the coefficient of variation of σ_B .

It should be noted that the relative variability of σ_B was used as an indirect indication of the presence of cap-shaped bubbles. This variability was estimated from time series as those shown in Figure 3, for sampling intervals that reduced the chances of autocorrelation. However, the relative variability in σ_B is only detected when the field of view is sufficiently small to observe the time instability (and spatial non-uniformity). Otherwise, the images should be split into several sub-images to conduct the image analysis. For fields of view much bigger than the cap-shaped bubbles, the average σ_B can also be in the range of normal conditions. In this work, the field of view was chosen to characterize BSDs in the spherical and spherical-ellipsoidal regimes, which also allowed the gas dispersion instability to be observed, given random sampling in the image processing.

Results from Figure 4 indicate that abnormal conditions are observed when $D_{32} > 6$ mm. However, these results were obtained by a semi-automated approach, in which irregular and cap-shaped bubbles were manually processed. The identification of these abnormal conditions from D_{32} estimates is then a time-consuming procedure. As most of BSD characterizations involve automated image processing, biased bubble size estimations may be significant in industrial practice. Irregular objects can also be detected by shape factors such as circularity or solidity; however, complex clusters also present low shape factors, hindering the detection of cap-shaped bubbles. The use of the relative variability of the shadow percentage is then a practical tool to detect abnormal conditions and to provide feedback to flotation operations. The technique implementation is straightforward, with low computational cost.

The abnormal conditions highlighted in Figure 4 correspond to BSDs measured in three first cells of rougher flotation banks and in two flotation columns. Insufficient frother conditioning time, damaged sparger, and lack of maintenance in the bubble generation systems were the main possible causes for the significant presence of cap-shaped bubbles in these flotation machines.

4. Conclusions

A straightforward image processing technique was proposed to detect abnormal gas dispersion conditions in flotation. This technique was based on the relative variability of the shadow percentage of binary images of bubble populations. The methodology was applied to industrial data from flotation cells and columns. The results showed that:

- The presence of cap-shaped bubbles caused peaks in the instantaneous shadow percentage, increasing its variability. This variability was significantly lower under spherical and spherical–ellipsoidal regimes.
- The relative variability of the shadow percentage justified part of the variability of the Sauter mean diameter. Under spherical and spherical–ellipsoidal regimes, a noisy increasing trend between the $cv_{\sigma B}$ and the D_{32} was observed.
- An abrupt increase in the coefficient of variation of the shadow percentage was observed in abnormal gas dispersion operations.
- A threshold of $cv_{\sigma B} \approx 80\%$ was determined as suitable to detect a significant presence of cap-shaped bubbles in flotation machines. From this threshold, $D_{32} > 6$ mm were observed.

The detection of cap-shaped bubbles from the relative variability of the shadow percentage is proposed to provide feedback to flotation processes. Thus, normal carrying capacities with nonsignificant disturbances at the pulp–interface can be monitored.

Author Contributions: Methodology, L.V. and J.Y.; software, L.V.; formal Analysis, L.V.; Writing—original draft preparation, L.V., J.Y., C.A. and I.C.; writing—review and editing, L.V., J.Y., C.A. and I.C.; supervision, L.V.; project administration, L.V. and J.Y.; funding acquisition, L.V. and J.Y. All authors have read and agreed to the published version of the manuscript.

Funding: Funding for process modeling and control research was provided by ANID, Project Fondecyt 1201335, and Universidad Técnica Federico Santa María, Project PI_LIR_2021_78.

Conflicts of Interest: The authors declare no conflict of interest.

References

1. Gorain, B.K.; Franzidis, J.P.; Manlapig, E.V. Studies on impeller type, impeller speed and air flow rate in an industrial scale flotation cell. Part 4: Effect of bubble surface area flux on flotation performance. *Miner. Eng.* **1997**, *10*, 367–379. [[CrossRef](#)]
2. Massinaei, M.; Kolahdoozan, M.; Noaparast, M.; Oliazadeh, M.; Yianatos, J.; Shamsadini, R.; Yarahmadi, M. Hydrodynamic and kinetic characterization of industrial columns in rougher circuit. *Miner. Eng.* **2009**, *22*, 357–365. [[CrossRef](#)]
3. Hernandez-Aguilar, J.R.; Rao, S.R.; Finch, J.A. Testing the k–Sb relationship at the microscale. *Miner. Eng.* **2005**, *18*, 591–598. [[CrossRef](#)]
4. Grau, R.A.; Laskowski, J.S. Role of frothers in bubble generation and coalescence in a mechanical flotation cell. *Can. J. Chem. Eng.* **2006**, *84*, 170–182. [[CrossRef](#)]
5. Guven, O.; Batjargal, K.; Ozdemir, O.; Karakashev, S.I.; Grozev, N.A.; Boylu, F.; Çelik, M.S. Experimental procedure for the determination of the critical coalescence concentration (CCC) of simple frothers. *Minerals* **2020**, *10*, 617. [[CrossRef](#)]
6. Cho, Y.-S.; Laskowski, J. Effect of flotation frothers on bubble size and foam stability. *Int. J. Miner. Process.* **2002**, *64*, 69–80. [[CrossRef](#)]
7. Castro, S.; Miranda, C.; Toledo, P.; Laskowski, J.S. Effect of frothers on bubble coalescence and foaming in electrolyte solutions and seawater. *Int. J. Miner. Process.* **2013**, *124*, 8–14. [[CrossRef](#)]
8. Gorain, B.K.; Napier-Munn, T.J.; Franzidis, J.-P.; Manlapig, E.V. Studies on impeller type, impeller speed and air flow rate in an industrial scale flotation cell. Part 5: Validation of k–Sb relationship and effect of froth depth. *Miner. Eng.* **1998**, *11*, 615–626. [[CrossRef](#)]
9. Vinnett, L.; Yianatos, J.; Arismendi, L.; Waters, K.E. Assessment of two automated image processing methods to estimate bubble size in industrial flotation machines. *Miner. Eng.* **2020**, *159*, 106636. [[CrossRef](#)]
10. Riquelme, A.; Desbiens, A.; Bouchard, J.; del Villar, R. Parameterization of Bubble Size Distribution in Flotation Columns. *IFAC Proc. Vol.* **2013**, *46*, 128–133. [[CrossRef](#)]
11. Fitzgibbon, A.W.; Pilu, M.; Fisher, R.B. Direct Least Squares Fitting of Ellipses. In Proceedings of the 13th International Conference on Pattern Recognition, Vienna, Austria, 25–29 August 1996; Volume 251, pp. 253–257.
12. Acuña, C.; Vinnett, L.; Kuan, S.H. Improving image analysis of online bubble size measurements with enhanced algorithms. In Proceedings of the 12th International Mineral Processing Conference (Procemin), Santiago, Chile, 26–28 October 2016.
13. The MathWorks Inc. *Image Processing Toolbox: User’s Guide*; The MathWorks Inc.: Natick, MA, USA, 2021.
14. Finch, J.A.; Dobby, G.S. *Column Flotation*; Pergamon Press: Oxford, UK, 1990.
15. Clift, R.; Grace, J.; Weber, M. *Bubbles, Drops, and Particles*; Academic Press: New York, NY, USA, 1978.
16. Yianatos, J.B.; Henríquez, F. Boundary conditions for gas rate and bubble size at the pulp–froth interface in flotation equipment. *Miner. Eng.* **2007**, *20*, 625–628. [[CrossRef](#)]
17. Vinnett, L.; Yianatos, J.; Alvarez-Silva, M. Gas Dispersion Measurements in Industrial Flotation Equipment. In Proceedings of the 8th Copper International Conference (Copper 2013), Santiago, Chile, 1–4 December 2013.

18. Hernandez-Aguilar, J.; Gomez, C.; Finch, J. A technique for the direct measurement of bubble size distributions in industrial flotation cells. In Proceedings of the 34th Annual Meeting of the Canadian Mineral Processors, Ottawa, ON, Canada, 22–24 January 2002; pp. 389–402.
19. Grau, R.A. An Investigation of the Effect of Physical and Chemical Variables on Bubble Generation and Coalescence in Laboratory Scale Flotation Cells. Ph.D. Thesis, Helsinki University of Technology, Helsinki, Finland, 2006.
20. Vinnett, L.; Alvarez-Silva, M. Indirect estimation of bubble size using visual techniques and superficial gas rate. *Miner. Eng.* **2015**, *81*, 5–9. [[CrossRef](#)]
21. Vinnett, L.; Yianatos, J.; Alvarez, M. Gas dispersion measurements in mechanical flotation cells: Industrial experience in Chilean concentrators. *Miner. Eng.* **2014**, *57*, 12–15. [[CrossRef](#)]